THE JOURNAL OF BIOLOGICAL CHEMISTRY
Vol. 272, No. 12, Issue of March 21, pp. 7817–7823, 1997
Printed in U.S.A.

Solution Structure of Toxin b, a Long Neurotoxin from the Venom of the King Cobra (*Ophiophagus hannah*)*

(Received for publication, October 1, 1996, and in revised form, December 16, 1996)

Shi-Shung Peng‡, Thallampuranam Krishnaswamy S. Kumar‡, Gurunathan Jayaraman‡, Chun-Chang Chang§, and Chin Yu‡¶

From the ‡Department of Chemistry, National Tsing Hua University, Hsinchu, Taiwan and the §Department of Biochemistry, Kaohsiung Medical College, Kaohsiung, Taiwan

The solution structure of toxin b, a long neurotoxin (73 amino acids and 5 disulfides) from the venom of *Ophiophagus hannah* (king cobra), has been determined using ^{1}H NMR and dynamical simulated annealing techniques. The structures were calculated using 485 distance constraints and 52 dihedral angle restraints. The 21 structures that were obtained satisfy the experimental restraints and possess good nonbonded contacts. Analysis of the converged structures revealed that the protein consists of a core region from which three finger-like loops extend outwards. The regular secondary structure in toxin b includes a double and a triple stranded antiparallel β sheet. Comparison with the solution structures of other long neurotoxins reveals that although the structure of toxin b is similar to those of previously reported long neurotoxins, clear local structural differences are observed in regions proposed to be involved in binding to the acetylcholine receptor. A positively charged cluster is found in the C-terminal tail, in Loop III, and in the tip of Loop II. This cationic cluster could be crucial for the binding of the long neurotoxins to the acetylcholine receptor.

Venom of snakes from the Elapidae and Hydrophyidae families possesses proteins with pronounced pharmacological activities (1, 2). Some of these proteins are potent cardiotoxins (3, 4), whereas others are postsynaptic neurotoxins (5–7). The neurotoxins are classified into two general groups, long and short neurotoxins (8, 9). Both classes of toxins bind specifically to the nicotinic acetylcholine receptor and block synaptic nerve transmission (10, 11). Binding of the neurotoxins to the acetylcholine receptor leads to a complete closure of the channel (11). The extremely tight, noncovalent association between the receptor and neurotoxins (K_d ranging from 10^{-9} to 10^{-11} M) in comparison with that of acetylcholine (K_d of 10^{-6} M) makes them useful tools with which to investigate the function of the neuromuscular synapse and its receptors (10, 12). The long and short neurotoxins exhibit sequence homology and similar overall topologies, characterized by a three stranded antiparallel β sheet and three finger-like loops protruding from a globular core (13). Long neurotoxins have four disulfide bridges like the short neurotoxins but possess an additional disulfide bridge in the central loop of the molecule. In addition to insertion and deletion within the main chain itself, long neurotoxins have an extra polypeptide chain between residues 65 and 73 that gives rise to a characteristic C-terminal tail (2). In long neurotoxins, the least conserved regions tend to be found in the C-terminal tail and the first loop (9). To date, x-ray and NMR structures of three long neurotoxins, namely α-cobratoxin (14, 15), α-bungarotoxin (16), and LSIII from *Laticauda semifasciata* (17), have been determined. The king cobra (*Ophiophagus hannah*), which belongs to the elapid family, is the world's largest poisonous snake (18). At least six long neurotoxin isoforms have been isolated from this venom source, and among these neurotoxin analogues, toxin b is the most toxic (18). Toxin b is 73 amino acids long and contains 5 disulfide bridges. In this paper, we report the solution structure of toxin b. We find that the overall fold of toxin b is similar to that of the other long neurotoxin structures. Consistent with previous studies, the secondary structure is characterized by an antiparallel double and a triple stranded β sheet conformation. However, subtle but important difference(s) are observed among the structures of α-cobratoxin (14, 15), α-bungarotoxin (16), and LSIII (17) with toxin b.

MATERIALS AND METHODS

NMR Experiments

Toxin b was purified from the *O. hannah* (king cobra) venom (Sigma) as described previously by Chang and co-workers (18). For all the NMR experiments, 38 mg of the toxin were dissolved in 0.5 ml of water (9 mM). The samples were prepared in two different ways to attain varied conditions for the exchange of the amide protons. A nonexchanged sample with all the amide protons was prepared by dissolving lyophilized toxin b in a mixture of H_2O (90%) and D_2O (10%) at 20 °C. The fully exchanged sample, yielding a spectrum without labile amide protons, was obtained by dissolving the protein in D_2O. The pH of the protein samples for NMR measurements was set at 3.0.

All NMR experiments were performed on a Bruker DMX-600 NMR spectrometer, and data were processed on a INDY work station using the UXNMR software. DQF-COSY[1] (19), total correlation spectroscopy (50 ms mixing time) (20), and DQ-COSY (21) spectra were collected for through-bond interactions. Water-gated NOESY (22) spectrum was acquired with a mixing time of 150 ms. In all NMR experiments, sodium 3-[*trimethylsilyl*-2,2,3,3-^{2}H]proponate was used as an internal standard.

Experimental Restraints

Distance Restraints—Inter-proton distance restraints, torsional angle restraints, and hydrogen bond restraints were derived from the NMR data. Intensities of the NOESY cross-peaks were classified into distances with three ranges, 0.18–0.27, 0.18–0.35, and 0.18–0.50 nm, corresponding to strong, medium, and weak NOE (23, 24). Distance

* This work was supported by Taiwan National Science Council grants NSC85-2311-B007-17 and NSC85-2133-M007-006. The costs of publication of this article were defrayed in part by the payment of page charges. This article must therefore be hereby marked "*advertisement*" in accordance with 18 U.S.C. Section 1734 solely to indicate this fact.

The atomic coordinates and structure factors (codes 1TXA and 1TXB) have been deposited in the Protein Data Bank, Brookhaven National Laboratory, Upton, NY.

¶ To whom correspondence should be addressed. Fax: 886-35-711082.

[1] The abbreviations used are: DQF-COSY, double quantum filtered correlated spectroscopy; DQ-COSY, double quantum correlated spectroscopy; NOE, nuclear Overhauser effect; NOESY, two-dimensional nuclear Overhauser enhancement spectroscopy; $^3J_{NH\alpha}$, vicinal spin-spin coupling constant between NH and the α proton; $^3J_{\alpha\beta}$, vicinal spin-spin coupling constants between the α-proton and β-protons.

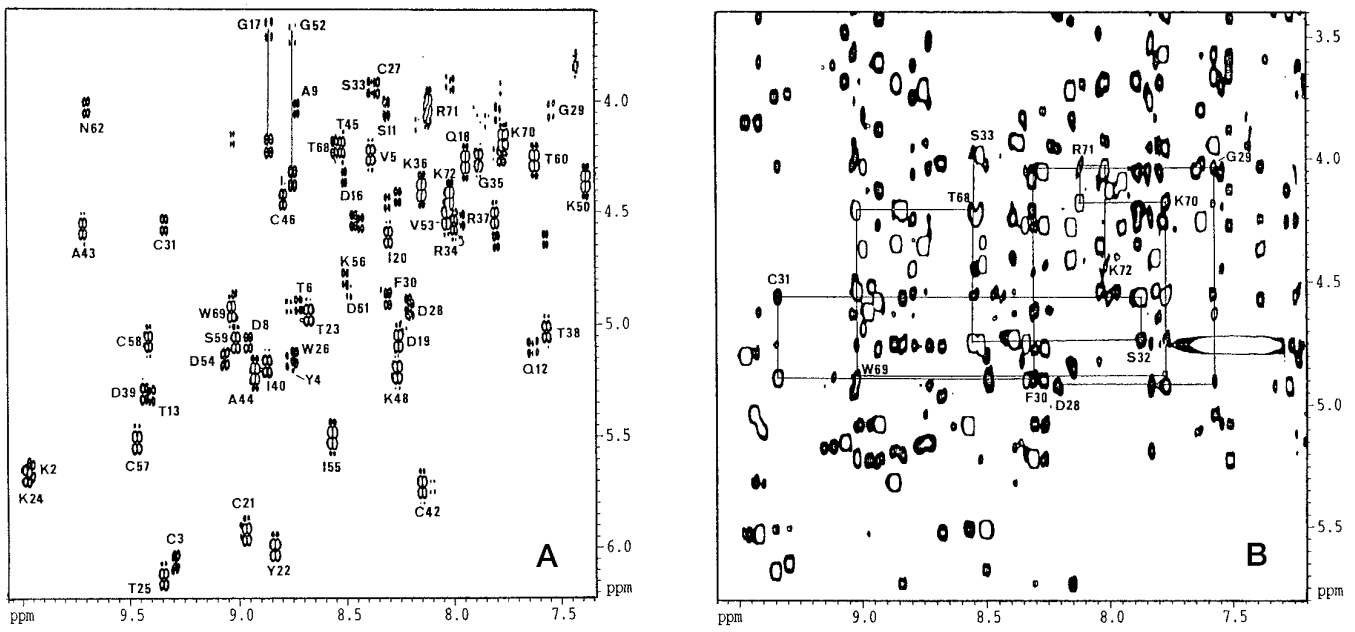

FIG. 1. **Fingerprint region of 600 MHz.** *A*, DQF-COSY spectrum of toxin b, pH 3.0, at 20 °C in 90% H_2O, 10% D_2O. Intra-residue cross-peaks (NH, $C^{\alpha}H$) are labeled. *B*, NOESY spectrum (150 ms mixing time) of toxin b, pH 3.0, at 20 °C in 90% H_2O, 10% D_2O. Sequential $H^{\alpha}{}_{(i)}$-$H^{N}{}_{(i+1)}$ connectivities for Asp^{28}-Ser^{33} and Thr^{68}-Lys^{72} are indicated by *connecting lines*.

restraints were explicitly used for the hydrogen bonds expected in the β sheet and consistent with the observed exchange rates and NOEs (25, 26). The hydrogen-deuterium exchange data for the backbone amide protons revealed that there are slowly exchanging amide protons in the secondary structure region.

Dihedral Angle Constraints—The $^3J_{NH\alpha}$ coupling constants were measured in the DQF-COSY spectra from cross-peak multiplets parallel to the ω_2 axis. The dihedral angle was restricted to the range of $-90°$, $-40°$ for $^3J_{NH\alpha}$ smaller than 5.5; for larger couplings with $^3J_{NH\alpha}$ greater than 10 Hz, the angle restraints were to the range of $-140°$, $-100°$ (27). Based on the above criteria, 38 backbone dihedral angle (ϕ) restraints were included in the structure calculation. Using analysis of the side chain coupling constants $^3J_{\alpha\beta}$ and intra-residue NOE, the χ_1 angle constraints were obtained (23). Stereospecific assignments were achieved on the basis of the $^3J_{\alpha\beta}$ coupling constants and the intra- and sequential inter-residue NOEs involving the amide, $C^{\alpha}H$, and $C^{\beta}H$ protons (28). In all, 14 prochiral centers were determined for the methylene protons on β carbons.

Three-dimensional Structure Calculations

The three-dimensional structures were calculated from the distance and angle constraints with a combination of the distance geometry and simulated annealing protocols using X-PLOR (29, 30). The target function contains several terms, one for bond lengths and bond angles, an improper torsional angular term, square well potential terms for NOE and restraints of torsional angles, and a soft repulsive term instead of van der Waals and electrostatic potentials (26). 50 initial structures were generated from a preliminary set of distance and angle constraints. The convergence of these initial structures was reasonable. The selection of the structures was based on the conditions that no distance constraints (per structure) exceeded 0.02 nm and that the NOE and total energies were minimal. The structure calculation is based on 485 distance constraints (158 long range, 50 medium range, and 101 sequential constraints, 36 for the backbone hydrogen bonding and 5 distance constraints for the disulfide bridges). Another 52 constraints of the dihedral angles were also included. The structures obtained upon distance geometry protocol were further refined by simulated annealing calculations using X-PLOR (30). To improve the ill-behaved structures, simulated annealing refinements were carried out on the energy-minimized structures. The refinement was based on satisfaction of each coordinate set in the family of generated structures. This is a slow cooling protocol with an additional feature of "softening" for van der Waals repulsion to enable atoms to move through each other. This routine consists of a 9-ps cooling dynamics followed by 200 cycles of Powell minimization. QUANTA (Molecular Simulations, Inc.) was used to generate, display, and analyze the structures.

RESULTS

Sequential Assignments—Almost all the protons in the protein have been assigned. The sequential resonance assignments were conducted following a well established method (31, 32). The DQ-COSY recorded in H_2O was of great value for unambiguous identification of glycine spin systems, since a remote peak is observed at $\omega_2 = \omega_{NH}$, $\omega_1 = \omega_{\alpha} + \omega_{\alpha 1}$ (21). These peaks were located in a specific well resolved region, and thus were easily identified. Identification of the $H^{\alpha}{}_{(i)}$-$H^{N}{}_{(i)}$ or $H^{\alpha}{}_{(i)}$-$H^{N}{}_{(i+1)}$ cross-peaks in the DQF-COSY and the NOESY spectra (mixing period, 150 ms) allowed for the sequential assignments in toxin b (Fig. 1). For most of the residues, the sequential NOE could be easily recognized, and in most cases, additional correlations with the protons of the side chain were also observed. According to the patterns of sequential NOEs observed for prolines, Pro^7, Pro^{15}, Pro^{65}, and Pro^{67} have been found to adopt the *trans* conformation.

The β protons of residues Asp^{16}, Asp^{19}, Cys^{21}, Asp^{28}, Phe^{30}, Cys^{31}, Ser^{32}, Asp^{39}, Cys^{42}, Cys^{57}, Cys^{58}, Ser^{59}, and Asn^{62} were stereochemically assigned following the criteria based on the values of the $^3J_{\alpha\beta}$ coupling constants and intra-residue NOEs (Fig. 2) (28, 29). The secondary structure elements in the protein were identified from the sequential and long range NOEs ($C^{\alpha}H$-$C^{\alpha}H$, NH-$C^{\alpha}H$, and NH-NH). Identification of the NOE between α protons of the backbone using the main chain-directed approach (33) also confirms the location of antiparallel double and triple stranded β sheets in the toxin (Fig. 3). The amide protons of most of the residues involved in the secondary structure formation are found to be protected from deuterium exchange. Residues Cys^{27}, Asp^{28}, Gly^{29}, and Phe^{30} form a type II turn. The other turns in the protein are not well characterized by the NOE constraints and do not fit into the classical types. In addition, medium range NOEs are observed between the $C^{\alpha}H$ of Cys^{27} and the NH of Gly^{35} and between the $C^{\alpha}H$ of Cys^{31} and the NH of Arg^{34}. These results suggest the presence of some local structure at the tip of Loop II. Similar types of NOEs were observed in the same region in α-cobratoxin and have been attributed to the presence of α helix (15). Interestingly, the exchange data show that the amide protons of Phe^{30},

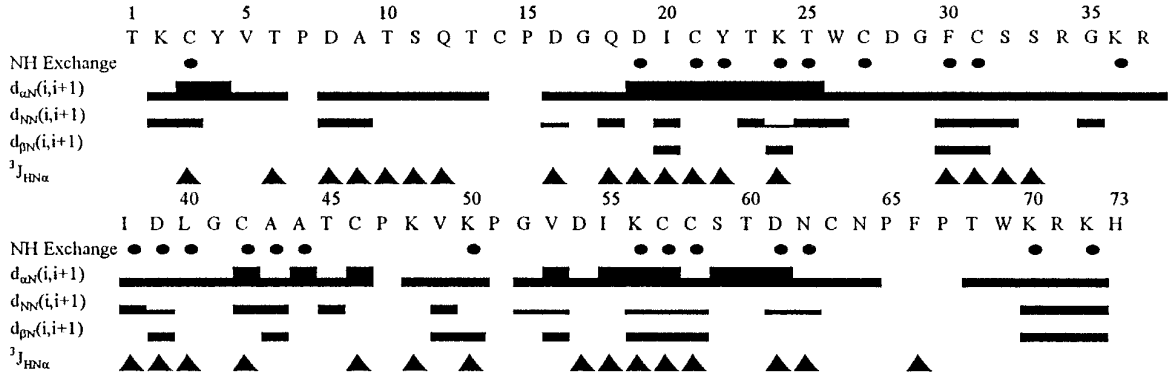

FIG. 2. **Amino acid sequence and survey of sequential NOE connectivities in toxin b.** Differences in NOE intensities of the sequential $d_{\alpha N}$, d_{NN}, and $d_{\beta N}$ connectivities are represented by *block height*. The *black circles* indicate the amide protons present in the DQF-COSY spectrum, which were recorded immediately after dissolving in D_2O at 10 °C.

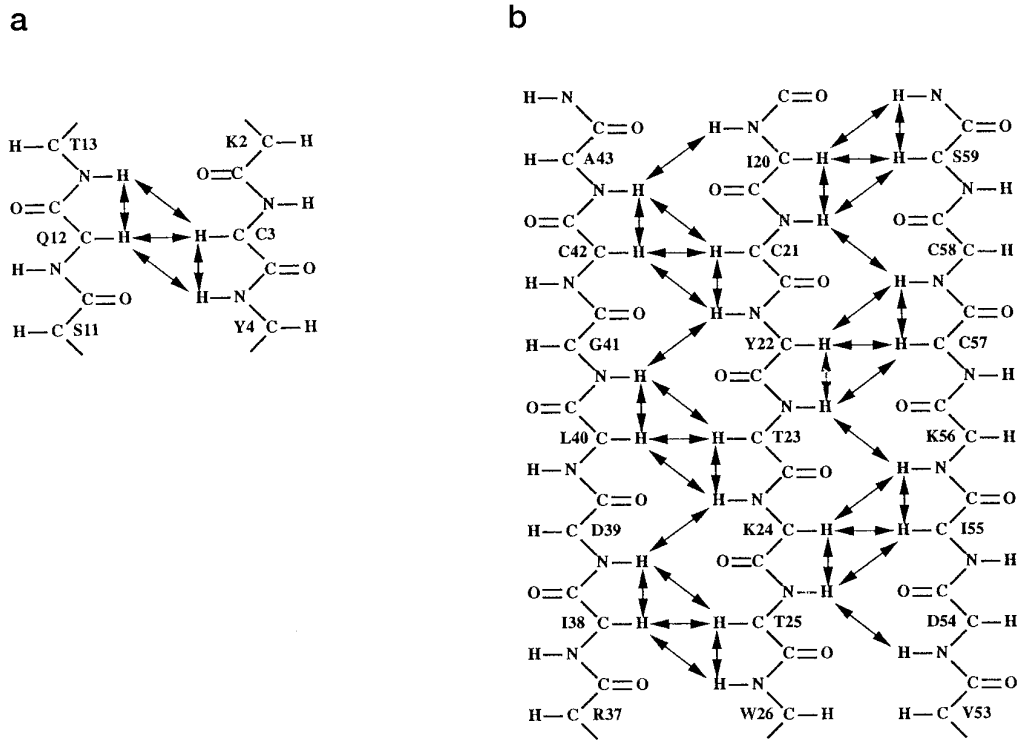

FIG. 3. **Main chain-directed pattern of toxin b.** *a*, double stranded region; *b*, triple stranded region. Proton pairs that generate NOE cross-peaks in the NOESY spectrum are indicated by the *double headed arrows*.

Cys^{31}, and Lys^{36} are protected from exchange (Fig. 2). This result gives an additional clue to the existence of local structure in this segment (residues 26–34) located at the tip of Loop II in toxin b. However, based on our NOE data we were unable to observe the helix conformation in this segment of toxin b. The NOE connectivity pattern in this segment does not satisfy all the criteria required for a typical helix.

Structure Determination—For the final calculation, 21 distance geometry structures were selected on the basis of their final error in the distance geometry calculations. These structures were calculated based on a total of 485 distance constraints (Fig. 4). The 21 structures were further refined with the simulated annealing protocol. The resultant structures were overlapped and are shown in Fig. 5. The energetic and geometric statistics of these refined structures are shown in Table I. All the structures are in good agreement with the experimental restraints, with no structure having a NOE restraint violation(s) greater than 0.2 Å or a dihedral angle restraint violation(s) greater than 4° (Fig. 5).

The Ramachandran plot for the average of 21 structures showed that the backbone dihedral angles of nearly all residues in the secondary structure segment(s) lie in the allowed regions (Fig. 6). Those residues that have unfavorable ϕ-ψ angles (backbone dihedral angles) were in poorly defined regions. Minimization of individual structures using CHARMm (33) gave negative Lennard-Jones energies (-291 ± 30 kcal/mol) with negligible shifts in atomic positions (backbone root mean square deviation < 0.15 Å), indicating favorable nonbonded interaction.

DISCUSSION

Structure Description—The three-dimensional structure of toxin b consists of three hairpin-type loops emerging from a globular head. Among the three loops, Loop I (Fig. 5, residues 1–14, *left loop*) and Loop III (residues 44–59, *right loop*) are shorter. Loop II (*middle loop*), comprising residues 19–43, is the longest. The sequence of residues 65–73 of the C-terminal end constitutes the tail of the molecule. The three loops are tethered together by four disulfide bridges, namely Cys^3-Cys^{21}, Cys^{14}-Cys^{42}, Cys^{46}-Cys^{57}, and Cys^{58}-Cys^{63}. The fifth disulfide

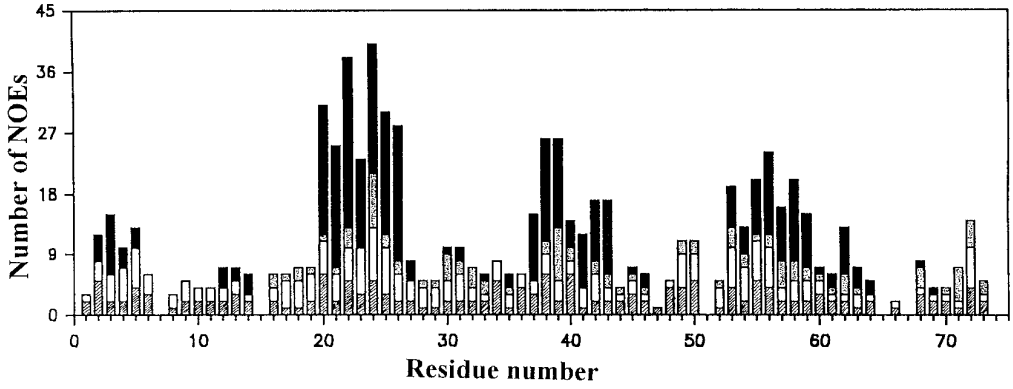

FIG. 4. **Sequence distribution of the NOE constraints used in the calculation of solution structures of Oh-8.** The various NOE constraints used in the structure calculation include intra-residual (*hatched*), sequential (*white*), medium range (*dotted*), and long range (*black*).

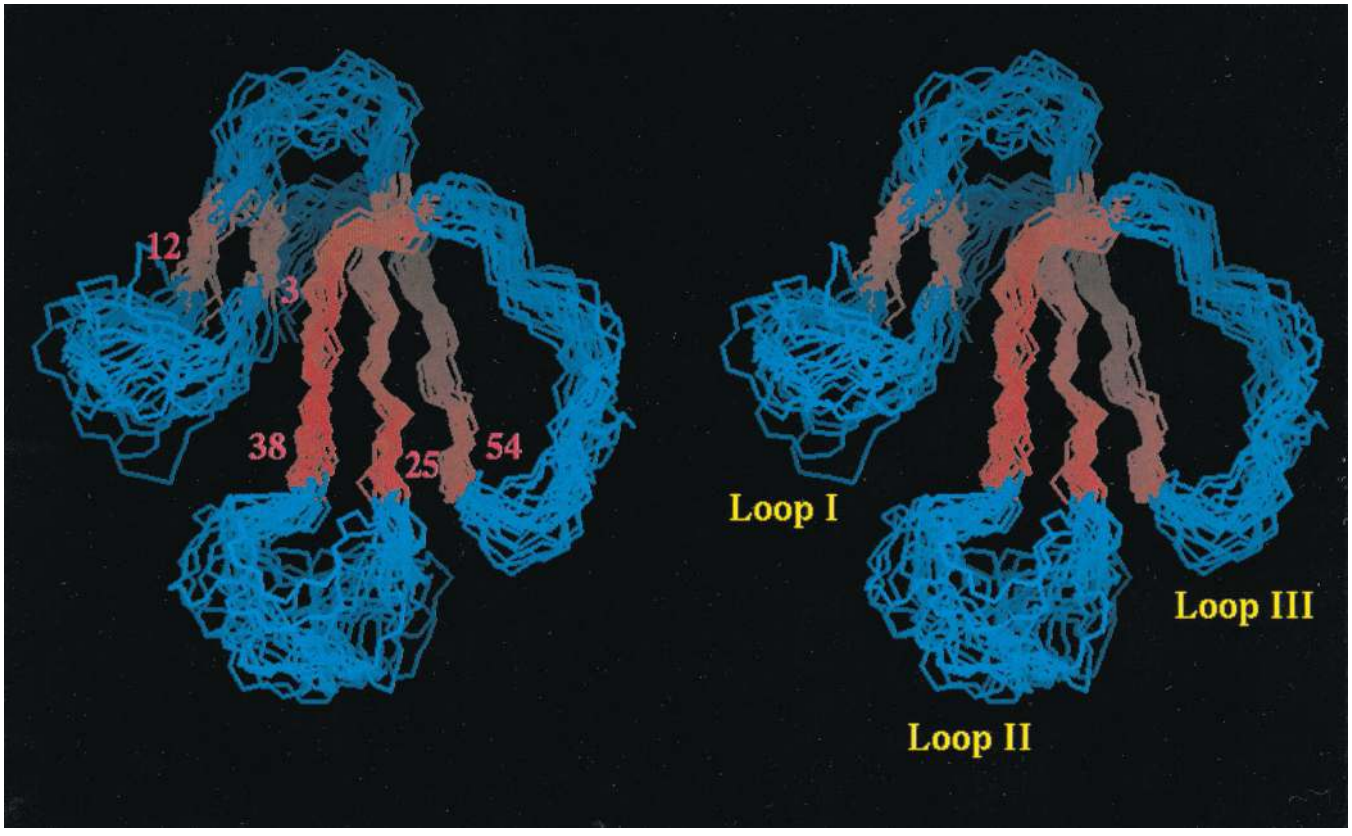

FIG. 5. **A stereo view of the best-fit superposition of the 21 NMR solution structures of toxin b as determined by dynamical simulated annealing calculations.** Residues 1–14 constitute Loop I, residues 19–43 constitute Loop II, and residues 44–59 constitute Loop III. The double and triple stranded β sheet segments are indicated in *red*. The residue *numbers* indicate the location of each of the β strands that make up the double and the triple stranded β sheet segments in the toxin.

bond from Cys^{27}-Cys^{31} is located at the lower tip of Loop II. Loop I involves two strands (strands 1 and 2) of the double stranded β sheet. The antiparallel double stranded β sheet in toxin b is very short, comprising residues 3–4 (strand 1) and 12–13 (strand 2). The double stranded β sheet are linked by a segment consisting of residues 4–11 (Fig. 5). It is internally stabilized by hydrogen bonding between residues 13 and 3. Loop I is partly hydrophobic (residues 2–5) and partly exposed to the solvent (residues 8–14). Loop II is the largest loop in the tertiary structure of all long neurotoxins; it consists of a narrow hairpin stem with a bulky tip that is stabilized in its structure by the disulfide bridge Cys^{27}-Cys^{31}. The stem portion lodges a part of the triple stranded antiparallel β sheet spanning residues 20–25 (in strand 3) and residues 38–43 in strand 4 (Fig. 5). Although the tip of Loop II appears mostly disordered, with high root mean square deviation values, a closer examination reveals some local order. The overlapped segment that constitutes the tip region (residues 26–34) showed a distorted right handed turn (Fig. 7). Such local structures have also been identified in the solution structures of both α-cobratoxin (15) and LSIII (17). The local structure in α-cobratoxin, however, has been designated as a "fluctuating" α helix (15). The structure in this region was found to be conformationally variable. The mobility is believed to be caused by the shortness of the helix (5 residues) and the high accessibility of the region to the solvent in α-cobratoxin. However, we believe that the nonavailability of the long range constraints could also account for the flexibility in this region of toxin b. Loop III of the molecule is stabilized by both the disulfide bridge between Cys^{46} and Cys^{57} and the type II β turn formed by Lys^{50}-Pro^{51}-Gly^{52}-Val^{53}. A portion of strand 5 that constitutes Loop III is involved in β sheet formation with Loop II and constitutes the triple strand

TABLE I
Structural statistics of Oh-8 from O. hannah
The values represent the average of the calculated 21 structures.

Root mean square deviations from idealized geometry	
Bond lengths (Å)	$(3.45 \pm 0.23) \pm 10^{-3}$
Bond angles (°)	0.769 ± 0.17
Dihedral angles (°)	1.288 ± 0.305
Energy term (kcal/mol)	
$E_{L\text{-}J}$[a]	-257 ± 30
E_{NOE}	41.98 ± 11.7
E_{edih}	4.96 ± 2.5
Root mean square deviations from the average NMR structure (for the backbone atoms)	
Triple stranded β sheet region (20–25, 38–43, 54–59)	0.678
Double stranded β sheet region (3–4, 12–13)	0.463
Loop II (26–34)	1.488
Residues 1–62	1.984
Residues 1–73	2.282

[a] L-J energy was calculated using the CHARMm 22 potential.

(Fig. 5). The tail at the C-terminal end is connected with Loop III by the disulfide bond between Cys^{58} and Cys^{63}. The C-terminal end of the molecule is found to be parallel to Loop II due to the formation of a type II β turn among residues 60–63. The C-terminal end tail comprising residues 65–73 is poorly defined by the available experimental data. There are very few long range constraints in this part of the molecule. The hydrophobic core of toxin b is well defined and is provided by residues that cluster around Tyr^{22}. The residues Lys^{24}, Leu^{40}, Ala^{43}, and Ala^{44} form a sort of cylinder from which the hydroxyl group of Tyr^{22} sticks out. In addition, Tyr^{4} along with Asn^{62}, Cys^{63}, and Asn^{64} lie close to the hydrophobic patch formed around Tyr^{22}.

Comparison with Other Long Neurotoxins—Toxin b shows reasonably high sequence homology with α-bungarotoxin (16), α-cobratoxin (15), and LSIII (17). Comparison of the solution structures of toxin b and the other long neurotoxins shows that the overall fold in all the toxins is similar (Fig. 8). The characteristic feature of all the long neurotoxins is the high flexibility of the tip portion of Loop II, as indicated by large root mean square deviations. The high flexibility could have a significant effect(s) on the thermodynamics and kinetics of ligand receptor binding of the long neurotoxins. The rate of association of the toxin to the acetylcholine receptor could increase, since the high flexibility of the loop could favor complex formation with the acetylcholine receptor by lowering the free energy barrier. The length of Loop II is the shortest in toxin b compared with that in α-cobratoxin, α-bungarotoxin, or LSIII (16–18). The length of this loop is believed to be intricately connected with the binding affinity of the neurotoxins to receptor (2). The longer the length of Loop II in the toxin, the greater is the affinity to the receptor (9). The structure of toxin b is strikingly different from that of the other long neurotoxins at the tip of Loop II. In both α-bungarotoxin (16) and α-cobratoxin (15) there is a distinct short nascent helix formed by the residues in segment 29–35. In toxin b, although there is local structure in the same region of Loop II, it could not be ascribed to a helical conformation (Fig. 7). Comparison of the solution structures of α-bungarotoxin, α-cobratoxin, LSIII, and toxin b reveals that except for the residues involved in the β sheet conformation, most portions of these long neurotoxin molecules are flexible (Fig. 8). The C-terminal tail region is poorly defined in all the long neurotoxins whose structures in solution have been studied. However, excision of the C-terminal tail by treatment with trypsin (34) and carboxypeptidase P (35) has been shown to have no effect on the structure of this toxin.

Possible Binding Region(s) of Neurotoxins to the Acetylcholine Receptor—Many residues located at the tip of Loop II are either strictly conserved or only conservatively substituted among short and long neurotoxins. Chemical modification studies have clearly demonstrated that many of the well conserved residues in Loop II have an important role in the toxicity of the long neurotoxins (9, 11, 12). Trp^{27} is conserved in all long and short neurotoxins (36). The indole ring of this conserved tryptophan is exposed to the solvent. Modification of Trp^{27} in a long neurotoxin analogue (Oh-4) from the king cobra venom showed a significant loss in the toxicity and acetylcholine binding efficiency of the toxin (37). Lys^{24} is yet another residue that is well conserved among the neurotoxins (5, 6). The neurotoxins are believed to interact with acetylcholine receptor through charge-charge interaction (11). It is postulated that the role of Trp^{26} is to orient the side chains of Lys^{24} and Asp^{28} residues at the tip of Loop II for effective binding to the acetylcholine receptor (38). In addition to Lys^{24}, the positive charge contributed by Arg^{34} is also believed to be important for the receptor binding (39). All the conserved residues in toxin b form a cluster at the tip of Loop II and thus may have a critical role in binding to the acetylcholine receptor. The disulfide bond holding Loop II has also been shown to be functionally important (40). Presumably, the cleavage of this disulfide bond disrupts the positively charged cluster at the tip of Loop II. In α-cobratoxin, the mobile lysine residue at position 49 has been postulated to have a role in the receptor binding (42). In erabutoxin b, it has been proposed that Loop II and Loop III together build a concave surface and that formation of such a surface promotes facile binding of the toxin to the receptor (5). Formation of such a concave surface(s) can also be seen in the GRASP representation of toxin b (Fig. 9). Neurotoxins are believed to bind to the acetylcholine receptor through multiple sites. In toxin a and α-bungarotoxin, the positively charged cluster formed by residues in Loop II (Arg^{34}, Arg^{37}), the C-terminal tail (Arg^{71}, Lys^{70}, Lys^{72}), and Loop III (Lys^{50}, Lys^{56}) is shown to be crucial for the receptor binding (41, 42). The positively charged cluster can also be visualized in the structure of toxin b (Fig. 9).

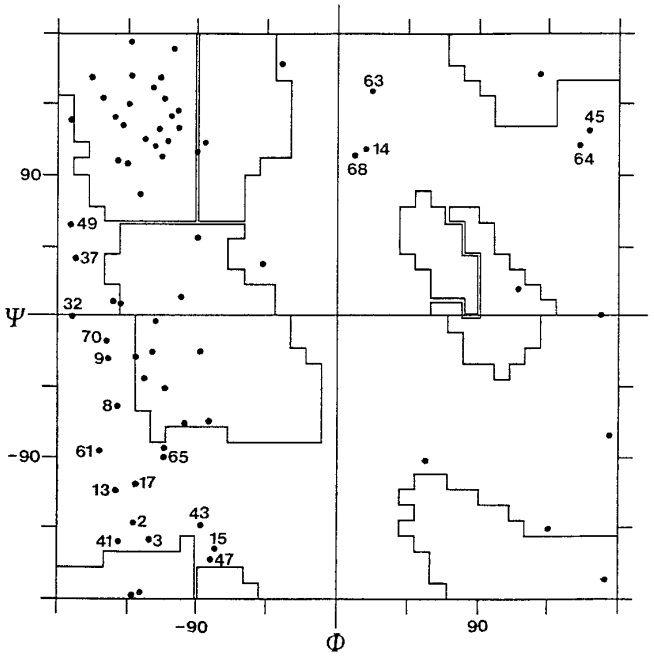

FIG. 6. **Ramachandran plot of the backbone conformational angles (ϕ-ψ) in the average structure (of 21 structures) of toxin b.** The residues that deviate from the allowed regions are indicated by *numbered dots*. These residues in unallowed regions are from the irregular segments of loops and turns that are not restricted by NMR constraints.

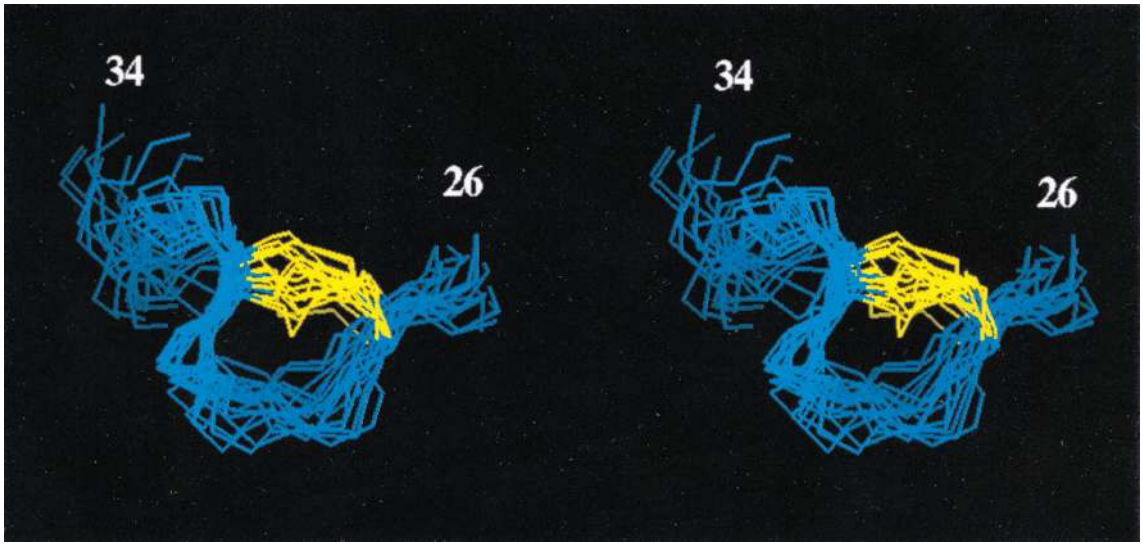

FIG. 7. **A stereo view of the least square superposition of N, C^{α}, and C′ of the 21 refined structures of toxin b at the tip of Loop II spanning residues 26–34.** This segment (residues 26–34) in the toxin shows a well defined local order.

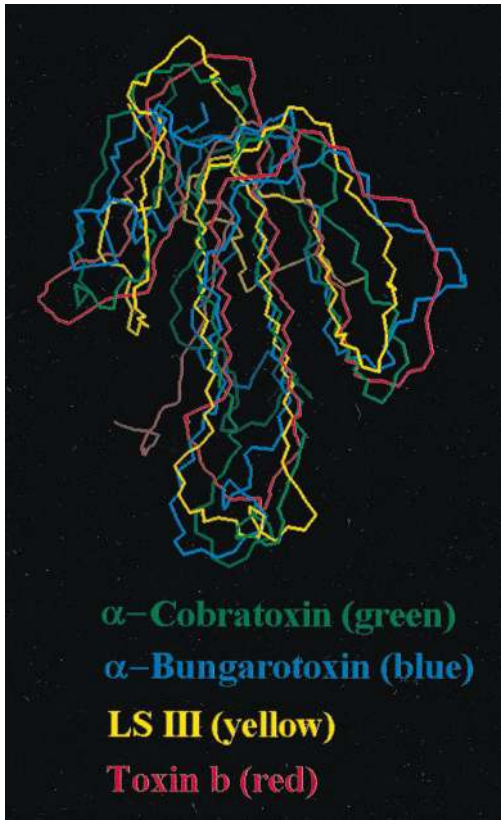

FIG. 8. **Superposition of backbone atoms of four toxin solution structures.** Mean structure of toxin b (*red*), α-bungarotoxin (*blue*), α-cobratoxin (*green*), and LSIII (*yellow*). All of the four long neurotoxins compared here show high root mean square deviations for residues not involved in the regular secondary structure.

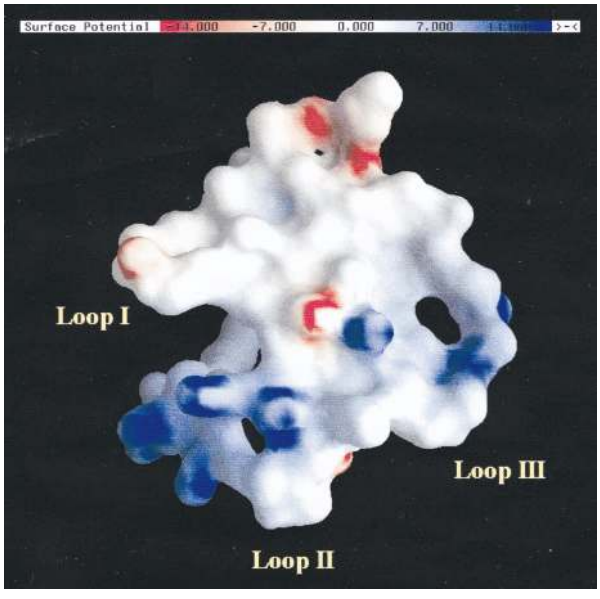

FIG. 9. **GRASP representation of the distribution of the positively (*blue*) and negatively (*red*) charged residues of toxin b.** The positively charged cluster constituted from cationic residues in the C-terminal tail, Loop III, and Loop II is involved in the binding of the toxin to the acetylcholine receptor.

Chemical modification of all the arginine and lysine residues belonging to the positively charged cluster leads to substantial loss in the antigenicity and receptor binding ability of the long neurotoxins (43–45). These results imply that the cationic centers located in Loops II and III and the C-terminal tail (Fig. 9) collectively contribute to the multipoint contact of the toxin to the acetylcholine receptor. The solution structure of toxin b thus reveals most of the structural features previously observed for the family of long neurotoxins. The tip of Loop II shows a prominent local order and, together with the cluster of positive charges formed by residues in the C terminus, Loop II, and Loop III, could constitute the active site involved in the acetylcholine receptor binding.

Acknowledgments—We acknowledge the Regional Instrumentation Center (Hsinchu, Taiwan) for allowing us to use the 600-MHz spectrometer.

REFERENCES

1. Harvey, A. L. (1985) *J. Toxicol. Toxin Rev.* **40,** 41–69
2. Dufton, M. J., and Hider, R. C. (1983) *CRC Crit. Rev. Biochem.* **14,** 113–171
3. Bhaskaran, R., Huang, C. C., Chang, D. K., and Yu, C. (1994) *J. Mol. Biol.* **235,** 1291–1301
4. Bhaskaran, R., Huang, C.-C., Tsai, Y.-C., Jayaraman, G., Chang, D.-K., and Yu, C. (1994) *J. Biol. Chem.* **269,** 23500–23508
5. Brown, L. R., and Wüthrich, K. (1992) *J. Mol. Biol.* **227,** 118–135
6. Basus, V. T., Song, G., and Hawrot, E. (1993) *Biochemistry* **32,** 12290–12298
7. Yu, C., Bhaskaran, R., Chaung, L. C., and Yang, C. C. (1993) *Biochemistry* **32,** 21312–21316
8. Yang, C. C. (1974) *Toxicon* **12,** 1–43
9. Mulac-Jericevic, B., and Atassi, M. Z. (1987) *Biochem. J.* **248,** 847–852
10. Changeux, J. P., Kasai, M., and Lee, C. Y. (1970) *Proc. Natl. Acad. Sci. U. S. A.* **67,** 1241–1247

11. Ruan, K. H., Stiles, B. G., and Atassi, M. Z. (1991) *Biochem. J.* **274,** 849–854
12. Rees, B., and Bilwes, A. (1993) *Chem. Res. Toxicol.* **6,** 385–406
13. Yu, C., Bhaskaran, R., and Yang, C. C. (1994) *J. Toxicol. Toxin Rev.* **13,** 291–315
14. Betzel, C., Lange, G., Pal, G. P., Wilson, K. S., Maelicke, A., and Saenger, W. (1991) *J. Biol. Chem.* **266,** 21530–21536
15. Goas, R. L., Laplante, S. R., Mikon, A., Delsuc, M. A., Guittet, E., Robin, M., Charpentier, I., and Lallemand, J. Y. (1992) *Biochemistry* **31,** 4867–4875
16. Basus, V. J., Billeter, M., Love, R. A., Stroud, R. M., and Kuntz, T. (1988) *Biochemistry* **27,** 2763–2771
17. Connolly, P. J., Stern, A. S., and Hoch, J. C. (1996) *Biochemistry* **35,** 418–426
18. Chang, C. C., Huang, T. Y., Kuo, K. W., Chen, S. W., Huang, K. F., and Chiou, S. H. (1993) *Biochem. Biophys. Res. Commun.* **191,** 214–223
19. Rance, M., Sorensen, O. W., Bodenhausen, G., Wagner, G., Ernst, R. R., and Wüthrich, K. (1983) *Biochem. Biophys. Res. Commun.* **113,** 967–974
20. Bax, A., and Davies, D. G. (1985) *J. Magn. Reson.* **65,** 335–360
21. Wagner, G., and Zuiderweg, G. R. P. (1983) *Biochem. Biophys. Res. Commun.* **113,** 854–860
22. Piotto, M., Saudek, V., and Skelnar, V. (1992) *J. Biomol. NMR* **2,** 661–665
23. Clore, G. M., Gronenborn, A. M., Brünger, A. T., and Karplus, M. (1985) *J. Mol. Biol.* **186,** 435–455
24. Williamson, M. P., Havel, T. F., and Wüthrich, K. (1985) *J. Mol. Biol.* **182,** 295–315
25. Wagner, G., Braun, W., Havel, T. F., Schaumann, T., and Wüthrich, K. (1987) *J. Mol. Biol.* **196,** 611–639
26. Driscoll, P. C., Gronenborn, A. M., Beress, L., and Clore, G. M. (1988) *Biochemistry* **28,** 2188–2198
27. Pardi, A., Billeter, M., and Wüthrich, K. (1984) *J. Mol. Biol.* **180,** 741–751
28. Hyberts, S. G., Marki, W., and Wagner, G. (1987) *Eur. J. Biochem.* **164,** 625–635
29. Nilges, M., Clore, G. M., and Gronenborn, A. M. (1988) *FEBS Lett.* **229,** 317–324
30. Brünger, A. T. (1992) *X-PLOR Software Manual, Version 3.1*, Yale University, New Haven, CT
31. Wüthrich, K. (1986) *NMR of Proteins and Nucleic Acids*, John Wiley & Sons, Inc., New York
32. Chazin, W. J., Rance, M., and Wright, P. E. (1988) *J. Mol. Biol.* **202,** 603–622
33. Englander, S. W., and Wand, A. J. (1987) *Biochemistry* **26,** 5953–5958
34. Wu, S. H., Chen, C. J., Tseng, M. J., and Wang, K. T. (1983) *Arch. Biochem. Biophys.* **227,** 111–121
35. Endo, T., Oya, M., Tamiya, N., and Hayashi, K. (1987) *Biochemistry* **26,** 4592–4596
36. Endo, T., and Tamiya, N. (1987) *Pharmacol. & Ther.* **34,** 403–451
37. Chang, C. C., Lin, P. M., Chang, L. S., and Kuo, K. W. (1995) *J. Protein Chem.* **14,** 89–94
38. Pillet, L., Tremeau, O., Ducancel, F., Drevet, P., Zinn-Justin, S., Pinkasfeld, S., Boulain, J.-C., and Menez, A. (1993) *J. Biol. Chem.* **268,** 909–916
39. Chicheportiche, R., Vincent, J. P., Kopeyan, C., Schweiz, H., and Lazdunski, M. (1975) *Biochemistry* **14,** 2081–2091
40. Martin, B. M., Chibber, B. A., and Maelicke, A. (1983) *J. Biol. Chem.* **258,** 8714–8722
41. Chang, C. C. (1994) *J. Chin. Biochem. Soc.* **23,** 83–90
42. Lin, S. R., Chi, S. H., Chang, L. S., Kuo, K. W., and Chang, C. C. (1996) *J. Protein Chem.* **15,** 95–101
43. Lin, S. R., and Chang, C. C. (1991) *Toxicon* **29,** 937–950
44. Lin, S. R., and Chang, C. C. (1992) *Biochim. Biophys. Acta* **1159,** 255–261
45. Lin, S. R., Chi, S. H., Chang, L. S., Kuo, K. W., and Chang, C. C. (1995) *J. Biochem.* **118,** 297–301